NANO LETTERS

pubs.acs.org/NanoLett Letter

Implantable Aptamer-Graphene Microtransistors for Real-Time Monitoring of Neurochemical Release in Vivo

Guangfu Wu, Nannan Zhang, Avi Matarasso, Ian Heck, Huijie Li, Wei Lu, J. Glenn Phaup, Michael J. Schneider, Yixin Wu, Zhengyan Weng, He Sun, Zan Gao, Xincheng Zhang, Stefan G. Sandberg, Dilruba Parvin, Elena Seaholm, Syed Kamrul Islam, Xueju Wang, Paul E. M. Phillips, Daniel C. Castro, Shinghua Ding, De-Pei Li, Michael R. Bruchas, and Yi Zhang*

Cite This: https://doi.org/10.1021/acs.nanolett.2c00289 Read Online

ACCESS | Metrics & More | Article Recommendations | Supporting Information

ABSTRACT: The real-time monitoring of neurochemical release *in vivo* plays a critical role in understanding the biochemical process of the complex nervous system. Current technologies for such applications, including microdialysis and fast-scan cyclic voltammetry, suffer from limited spatiotemporal resolution or poor selectivity. Here, we report a soft implantable aptamer-graphene microtransistor probe for real-time monitoring of neurochemical release. As a demonstration, we show the monitoring of dopamine with nearly cellular-scale spatial resolution, high selectivity (dopamine sensor >19-fold over norepinephrine), and picomolar sensitivity, simultaneously. Systematic benchtop evaluations, *ex vivo* experiments, and *in vivo* studies in mice models highlight the key features and demonstrate the capability of capturing the dopamine release dynamics evoked by pharmacological stimulation, suggesting the potential applications in basic neuroscience studies and studying neurological disease-related processes. The developed system can be easily adapted for monitoring other neurochemicals and drugs by simply replacing the aptamers functionalized on the graphene microtransistors.

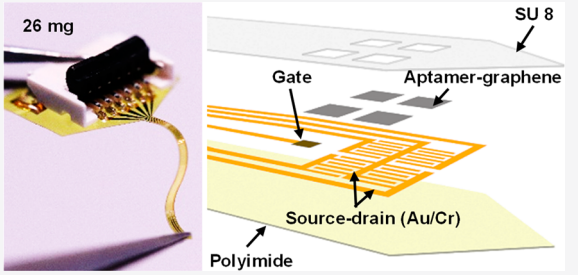

KEYWORDS: *graphene microtransistors, neurochemical sensors, real-time monitoring, dopamine*

INTRODUCTION

The human central nervous system contains billions of neurons that communicate through the propagation of action potentials along the cell membrane and the release, transport, and metabolism of neurochemicals at the synapses. Technologies for *in vivo* electrophysiology have been intensively studied, with recent examples of Neuropixels 2.0[1] and Neural Matrix[2] for recording over several thousand channels. Compared with these tools for electrophysiological recordings, the technologies for real-time neurochemical monitoring are very limited. Neurochemicals, however, have been found to play critical roles in reward signaling,[3] learning,[4,5] motor control,[6] and treatments of neurological disorders, such as Parkinson's disease, schizophrenia, and Alzheimer's disease.[7−9] Current technologies for neurochemical monitoring include microdialysis or fast-scan cyclic voltammetry (FSCV);[10−14] microdialysis probes have limited spatial and temporal precision due to the large probe size (150−440 μm in diameter)[15] and relatively low sampling rate (typically several minutes, though microdialysis with 1 min temporal resolution has been reported[16]), while the FSCV is limited by molecular specificity (Table S1). Similarly, the recently developed organic electrochemical transistor arrays that rely on the oxidation reaction of redox-active dopamine on the surface of the gate electrode cannot distinguish structurally similar neurochemicals[17] (Table S1).

Recently, Andrews et al. reported an implantable aptamer functionalized In_2O_3 field-effect transistor for monitoring serotonin *in vivo*.[18] Compared with In_2O_3 used in this study, graphene has a much higher carrier mobility than that of In_2O_3 (17.8 ± 1.8 $cm^2/V{\cdot}s$).[18,19] In addition, graphene offers many attractive properties for *in vivo* biosensing applications, such as biocompatibility and chemical inertness.[20−23] The graphene microtransistor is a three-terminal electronic device in which graphene is used as a channel material between the source and drain terminals.[23] While graphene microtransistors have been used for electrophysiological recordings *in vivo*[24−26] and the detection of dopamine *in vitro*,[27,28] there is no study to date on the real-time monitoring of dopamine release *in vivo* using implantable aptamer modified graphene microtransistors.

Received: January 22, 2022
Revised: April 9, 2022

https://doi.org/10.1021/acs.nanolett.2c00289
Nano Lett. XXXX, XXX, XXX−XXX

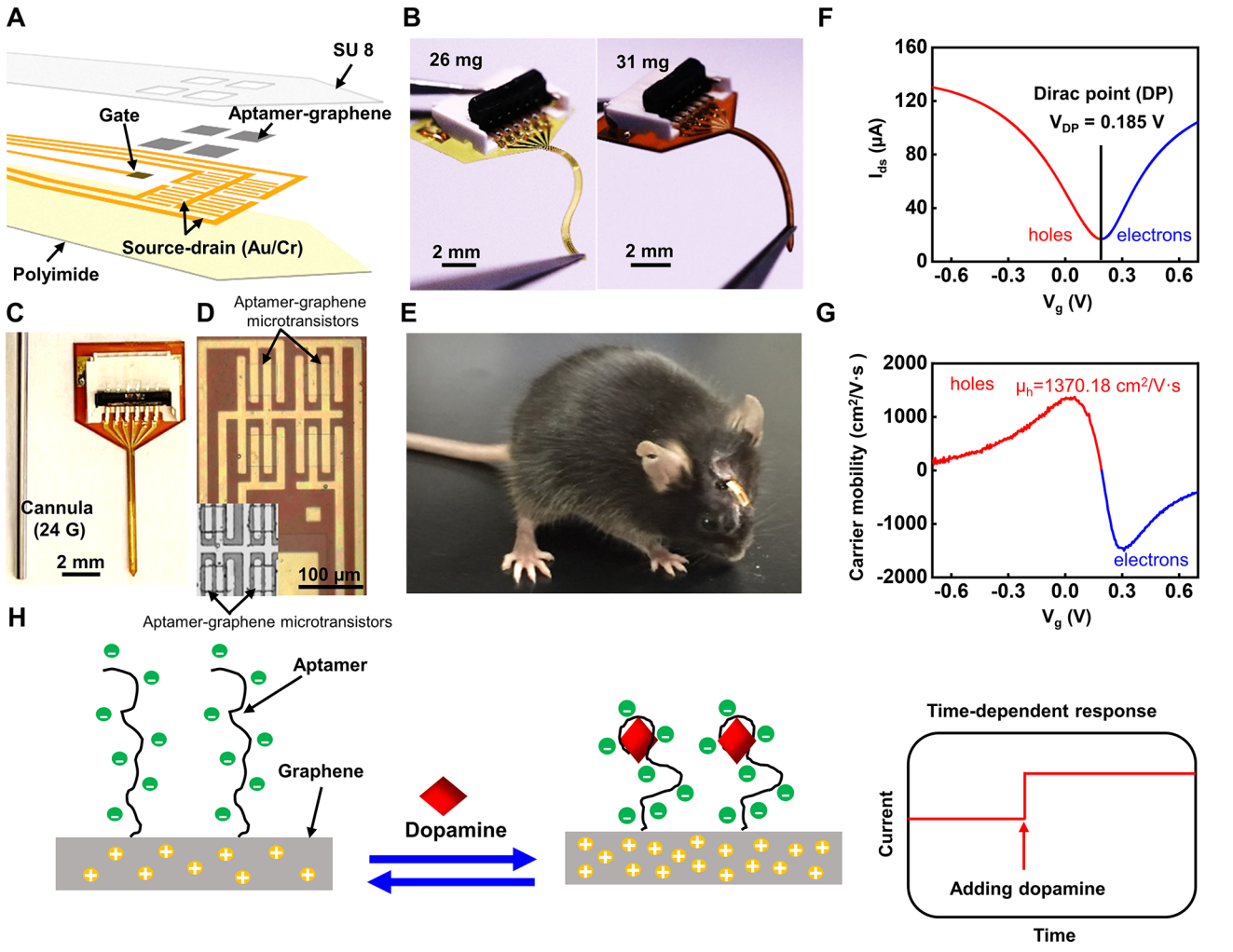

Figure 1. Design, fabrication, and working principle of implantable aptamer-graphene microtransistor probe for neurochemical monitoring. (A) Schematic illustration and (B) Optical images of the implantable aptamer-graphene microtransistor probe fabricated on (left) 7.6 μm PI (26 mg) and (right) on 76 μm PI (31 mg) for neurochemical monitoring. (C) Comparison of a conventional metal cannula (left, 24 gauge) and an implantable aptamer-graphene microtransistor probe (Right). The filament neural probe (~390 μm wide, ~76.8 μm thick) consists of four aptamer-graphene microtransistors, with each microtransistor at a nearly cellular-scale dimension (50 μm × 50 μm). (D) Optical and scanning electron microscope (inset) images of the tip end of an implantable aptamer-graphene microtransistor probe. (E) Image of a freely moving mouse implanted with an aptamer-graphene microtransistor probe. (F) A representative transfer curve of aptamer-graphene microtransistors. V_{ds} = 100 mV. (G) Gate voltage-dependent carrier mobility of aptamer-graphene microtransistors. (H) The working principle of aptamer-graphene microtransistor probe to monitor dopamine. The binding of dopamine induces a structural rearrangement of the dopamine aptamer, resulting in a p-doping effect (right-shift) on the graphene channel and an increase of source-drain current.

Here, we report an implantable aptamer-graphene microtransistor probe that enables the real-time monitoring of dopamine with nearly cellular-scale spatial dimension, high selectivity, and picomolar sensitivity, simultaneously. This neural probe successfully captures the dopamine release with pharmacological stimulation *in vivo* in small animal models of mice.

RESULTS

Design and Fabrication of Implantable Aptamer-Graphene Microtransistor Probe. We designed an implantable filament probe (~390 μm wide, ~76.8 or 8.4 μm thick) that consists of four aptamer-functionalized graphene microtransistors (Figure 1A–D and Figure S1), with each graphene microtransistor at a nearly cellular-scale dimension (50 μm × 50 μm). We chose this array design due to the heterogeneous release of dopamine.[29,30] This array design also offers the possibility for multiplex neurochemical monitoring. The aptamer functionalized graphene microtransistors couple the highly specific aptamers with ultrasensitive graphene microtransistors for real-time monitoring of neurochemicals. Aptamers are highly selective to targeted molecules. They can also conquer the Debye screening limitation of graphene microtransistors.[31] Furthermore, compared with other bioreceptors, aptamers possess several advantages, including high selectivity toward the target of interest, high stability, and long shelf life in harsh conditions.[32,33]

While the overall probe width is ~390 μm, the size of each graphene microtransistor defines the monitoring spatial resolution. This spatial resolution (50 μm × 50 μm) is much smaller than that of the microdialysis probe (150–440 μm in diameter; length of 1–4 mm),[15] affording neurochemical sensing high spatial resolution. Moreover, the small size of each aptamer-graphene microtransistor enables spatially precise,

https://doi.org/10.1021/acs.nanolett.2c00289
Nano Lett. XXXX, XXX, XXX−XXX

nearly cellular-scale monitoring of neurochemicals with reduced tissue damage and inflammation for *in vivo* uses. Figure 1B shows that the aptamer-graphene microtransistors can be fabricated on polyimide substrates with different flexibility. Considering the need of a surgical shuttle for 8.4 μm thick aptamer-graphene microtransistor probe in *in vivo* applications, in this study, we used aptamer-graphene microtransistors with a thickness of 76.8 μm; such a thickness offers sufficient mechanical stiffness for the device implantation while providing adequate mechanical flexibility to minimize the irritation at the device−tissue interfaces.[34] The soft mechanics (76.8 μm thick, bending stiffness of ~5.89 × 10^{-8} N·m^2, a value that is 3 orders of magnitude lower than the stiffness of the smallest optical fiber, which is 1 × 10^{-5} N·m^2[35]) and light weight (31 mg) of the implantable graphene microtransistor probe allow for implantation into the deep brain of small animals, such as mice, with reduced tissue damage and formation of glial scars due to micromotions of implants[36] (Figure 1B and E).

Figure 1F shows a representative V-shaped transfer curve of the aptamer-graphene microtransistor. The type of charge carriers of the graphene microtransistors can be tuned from holes (left branch) to electrons (right branch), resulting in an "ambipolar behavior". The carrier mobility (μ) in the linear region of the transfer curve is determined by two key parameters: (1) the total gate capacitance C_{TG} and (2) $\partial I_{ds}/\partial V_g$ (commonly called transconductance, g_m)

$$\mu = \frac{\partial I_{ds}}{\partial V_g} \cdot \frac{l}{w} \cdot \frac{1}{C_{TG} \cdot V_{ds}} \quad (1)$$

in which I_{ds}, V_g, l, w, and V_{ds} are drain-source current, gate voltage, graphene channel length, graphene channel width, and drain-source voltage, respectively. By calculating gate-dependent carrier mobility, a gate voltage of 50 mV affords the highest hole mobility (1370.18 cm^2/V·s) which was used in the following experiments (Figure 1G).

Working Principle of Implantable Aptamer-Graphene Microtransistors. The binding of dopamine to aptamer causes a conformational change of the aptamer that anchors on the graphene surface, resulting in the increase/decrease of carriers (electrons or holes) in the graphene channel and the generation of a measurable change in the source-drain current (I_{ds}) of aptamer-graphene microtransistors (Figure 1H). This current change is proportional to the target concentration. To quantify the sensing performance of implantable aptamer-graphene microtransistors for monitoring dopamine, the I_{ds} was recorded (the graphene microtransistors were biased at 100 mV source-drain voltage and a gate voltage of 50 mV was applied) when the probes were exposed to the targeted neurochemical with various concentrations. The electrical response in this study is defined as $\Delta I_{ds}/I_0$, where ΔI_{ds} and I_0 are the change of the source-drain current in the presence of dopamine and the initial signal without the dopamine, respectively. The current modulation is expressed as a function of the change in the carrier density (Δn) in the graphene channel, which is proportional to the number of targets (N) captured by the aptamer[37,38]

$$\Delta I_{ds} = \frac{w}{l} \cdot e \cdot \mu \cdot V_{ds} \cdot \Delta n \propto N \quad (2)$$

where w is the width of the graphene channel; l is the length of the graphene channel; e is the elementary charge (1.602 × 10^{-19} C); μ is the carrier mobility; and V_{ds} is the source-drain voltage.

Real-Time Monitoring of Dopamine. The dopamine aptamer, reported by a previous study,[31] was functionalized onto the graphene surface through $\pi-\pi$ stacking by a pyrene group, which was inserted into the 5′-end of the aptamer during the aptamer synthesis process.[37] Surface functionalization of graphene with dopamine aptamers causes a right shift of the Dirac point (V_{DP}) of transfer curves (Figure 2A and B),

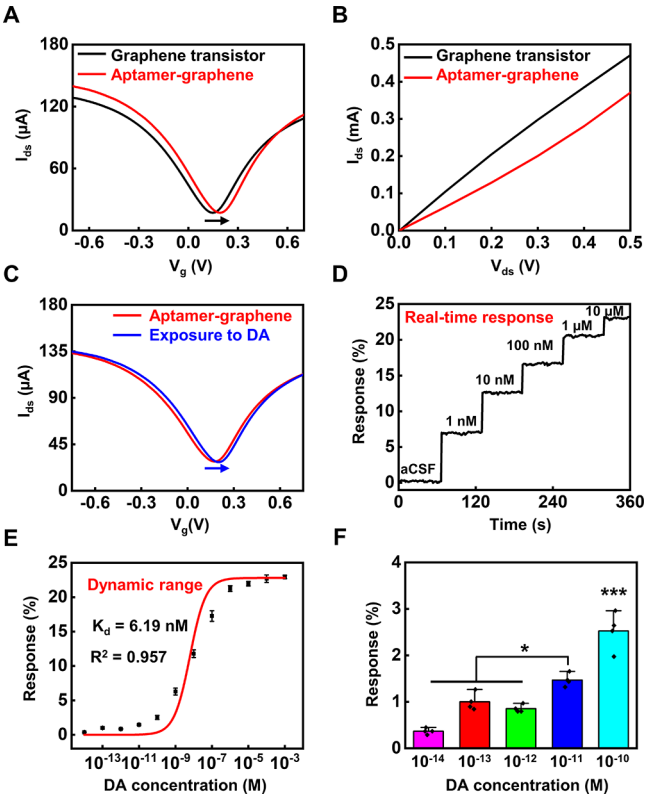

Figure 2. Real-time monitoring of dopamine with implantable aptamer-graphene microtransistor probe. (A) Transfer characteristics of graphene microtransistors functionalized with dopamine aptamer. (B) $I-V$ curves of graphene microtransistors and dopamine aptamer functionalized graphene microtransistors. (C) Transfer characteristics of a representative dopamine sensor before and after exposure to dopamine. DA: dopamine. (D) The real-time current response of the aptamer-graphene microtransistors upon exposure to aCSF solution containing dopamine with different concentrations. The probe was biased at 100 mV (V_{ds}), and a gate voltage (V_g) of 50 mV was applied. (E) The responses of dopamine sensors for monitoring dopamine from 10 fM to 1 mM (n = 3). (F) The responses when the dopamine sensor was exposed to dopamine with low concentrations (10 fM, 100 fM, 1 pM,10 pM, and 100 pM). ***p < 0.001, *p < 0.05.

which is attributed to the attachment of the negatively charged aptamer on the graphene surface and the resulting increase of hole carrier density due to the electrostatic effect.

A positive shift of the transfer curve is observed after the exposure of the dopamine sensor to dopamine (Figure 2C), suggesting that more hole carriers are induced on the graphene channel due to the conformational change of aptamer in the presence of dopamine. With a fixed gate voltage of 50 mV, the electrical current of aptamer-graphene microtransistors increases with the increase of dopamine concentration (Figure 2D). For sensitivity, the dopamine sensor shows a limit of

https://doi.org/10.1021/acs.nanolett.2c00289
Nano Lett. XXXX, XXX, XXX−XXX

detection in aCSF of 10 pM (Figure 2E and F, $p < 0.05$), attributed to the high carrier mobility of graphene. The dopamine sensor shows a dynamic range of 10 pM to 100 μM. The relationship between the electrical response of the dopamine sensor and dopamine concentration can be modeled by the Langmuir adsorption isotherm,[37] in which K_d represents the equilibrium dissociation constant that can indicate the binding affinity of the aptamer−target complex. The dopamine sensor shows a K_d of 6.19 nM (Figure 2E), indicating a high affinity of the aptamer toward dopamine.

Reversibility and Temporal Resolution of Implantable Aptamer-Graphene Microtransistor Probe. We find that the responses of dopamine sensors are reversible, as verified by recording the electrical response for changing the concentration of dopamine in aCSF (Figure 3A and B). The dopamine sensors show continuous signal-on and signal-off after exposure to the target with various concentrations and the subsequent aCSF buffer solution. The electric response switches on after the dopamine binding (from 1 nM to 10 μM), while the response switches off after the exposure to fresh aCSF buffer solution (95% recovery). Subsequently, the response turns on after exposure to dopamine again (1 nM and 10 μM, >95% recovery) (Figure 3B). This reversible response is attributed to the reversible conformational rearrangement of aptamer upon the binding to dopamine.[39] The reversible response of the aptamer-graphene microtransistor involves multiple recognition events rather than a single sensing event which is commonly observed for antibodies, allowing for monitoring local neurotransmitter and stimulation-evoked neurotransmitter release *in vivo*. The response time was measured by immersing the aptamer-graphene microtransistors into microchambers containing dopamine solution with different concentrations. The dopamine sensor exhibits a rapid dynamic response when the target concentration is changed; the probes reached 95% peak response within 2.09 s on time when increasing dopamine concentration from 10 nM to 100 nM and then returned to within 95% of the baseline when decreasing dopamine concentration back to 10 nM by 5.38 s off time (Figure 3C). Nevertheless, future work on tuning the aptamer-dopamine affinities and aptamer-dopamine kinetics, through changing stem lengths[31] and stem destabilization,[40] is needed to push the temporal resolution down to subsecond scale.

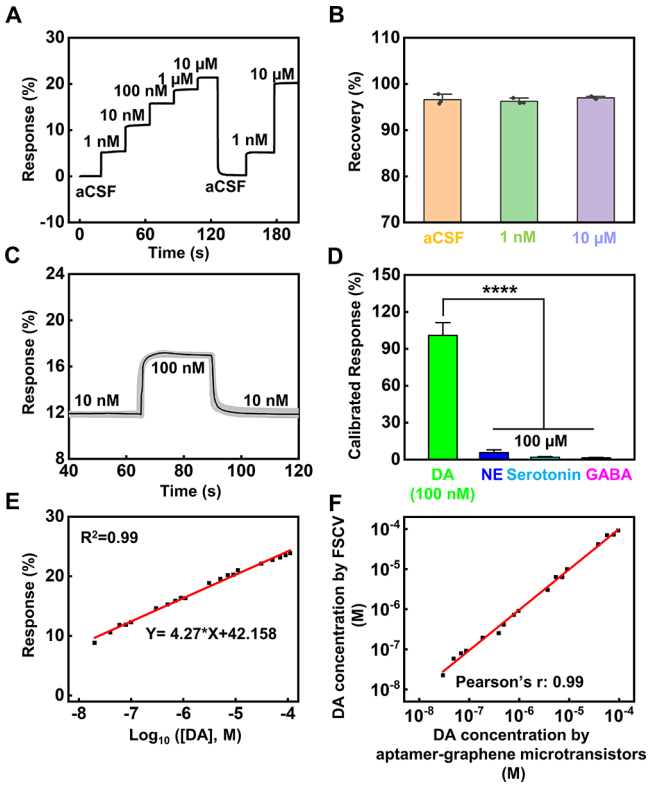

Figure 3. Reversibility, response time, selectivity, and benchmarking of implantable aptamer-graphene microtransistor probe. (A) Reversible response of dopamine sensors when the probes were exposed to aCSF solution and the dopamine with different concentrations. (B) The signal recovery of dopamine sensors. (C) Temporal response of the probe to dopamine. The probe was exposed to 10 nM dopamine, then 100 nM, and finally 10 nM to calculate the response time reaching 95% of peak response or baseline response. (D) Selectivity of dopamine sensors. Dopamine samples were kept at 100 nM. The concentration of other neurotransmitters as the interfering group was 3 orders of magnitude higher, which was 100 μM. DA: Dopamine. NE: Norepinephrine. GABA: Gamma-aminobutyric acid. Results are given as mean ± standard derivation (SD), $n = 3$, ****$p < 0.0001$. (E) The calibration curve between electrical response and dopamine concentration. (F) Comparison of dopamine concentration in aCSF measured from calibrated dopamine sensor with those obtained from FSCV carbon fiber electrode.

Selectivity of Implantable Aptamer-Graphene Microtransistor Probe. To investigate the molecular specificity of aptamer-graphene microtransistors for dopamine detection, the electrical response was recorded when exposed to different neurochemicals such as dopamine (DA), serotonin, norepinephrine (NE), and gamma-aminobutyric acid (GABA) (Figure 3D). A significantly higher response (17.29%) is observed when the dopamine sensors were exposed to dopamine (100 nM) compared to the exposure to 3 orders of magnitude higher concentrations (100 μM) of NE (0.91%), serotonin (0.31%), and GABA (0.23%). Thus, the dopamine sensor is less sensitive to 100 μM norepinephrine (NE), serotonin, and GABA than to 100 nM dopamine by factors of 19, 56, and 75, respectively.

Comparison and Benchmarking of Implantable Aptamer-Graphene Microtransistor Probe. The overall comparison between implantable aptamer-graphene microtransistors and other representative techniques for *in vivo* neurochemical monitoring can be found in Table S1. When compared with the FSCV,[41] organic electrochemical transistor,[17] and genetically encoded fluorescent sensors,[30,42] it offers an at least 100-fold improvement of sensitivity. It also provides the capability to distinguish structurally similar neurochemicals such as dopamine and norepinephrine. This spatial precision and selectivity are comparable to the state-of-the-art genetically encoded fluorescent sensors,[30,42] which, however, require complicated genetic encoding of neurons and a fluorescent imaging system (fiber photometry or fluorescence microscope) for the signal recording. The aptamer-graphene microtransistors show the response time on the order of seconds (2.09 s on time and 5.38 s off time), compared with subsecond or milliseconds temporal resolution of genetically encoded fluorescent sensors and FSCV.

To further benchmark and evaluate the accuracy of implantable aptamer-graphene microtransistors, the as-prepared dopamine sensor was first calibrated in aCSF solution containing physiologically relevant concentrations of dopamine (Figure 3E). Then we used both calibrated aptamer-graphene

https://doi.org/10.1021/acs.nanolett.2c00289
Nano Lett. XXXX, XXX, XXX−XXX

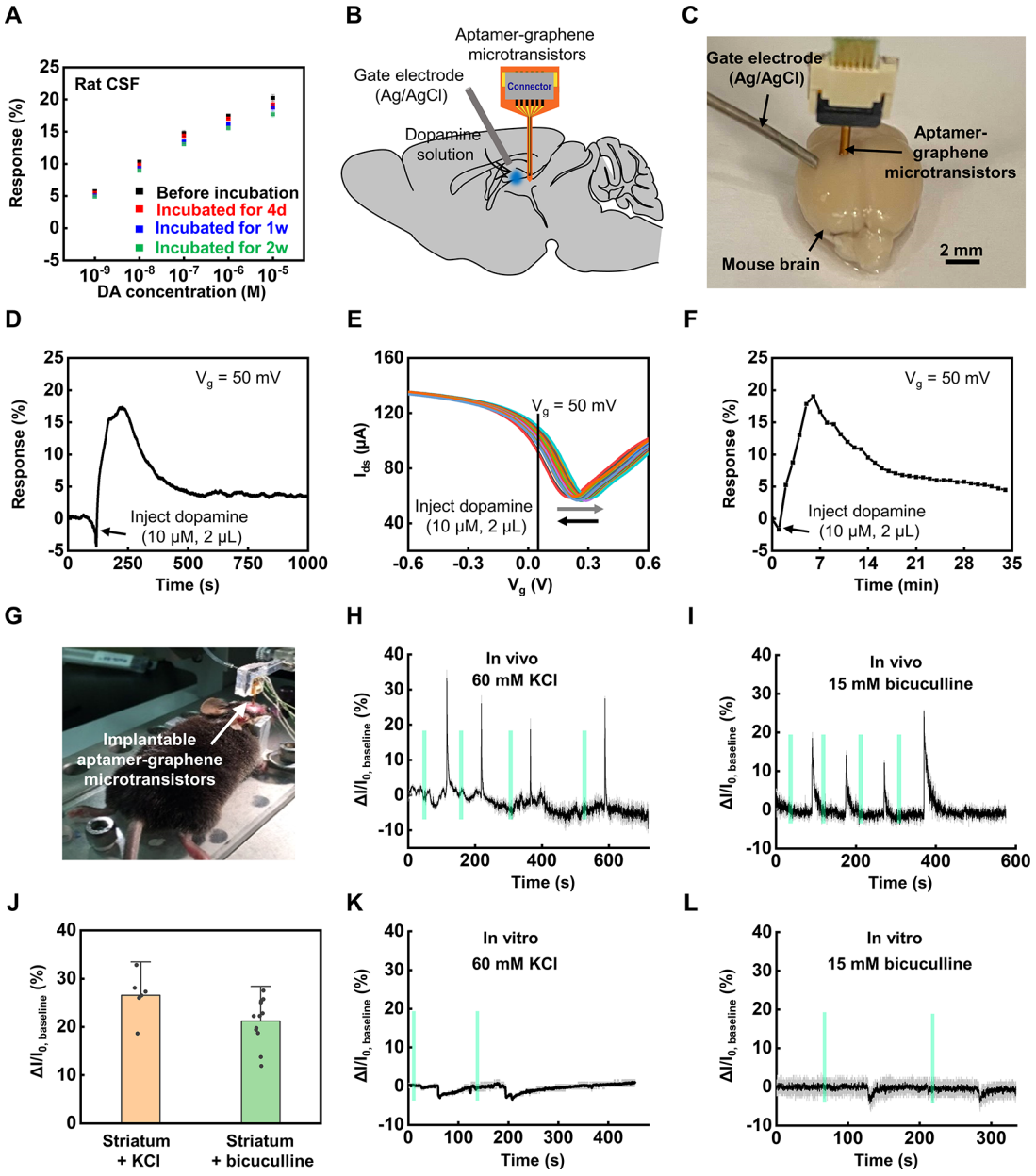

Figure 4. Stability in CSF, *ex vivo* studies in harvested mouse brain tissue, and real-time monitoring of dopamine release with pharmacological stimulation *in vivo* in the striatum of mice. (A) The stability of implantable aptamer-graphene microtransistors in rat CSF (BioIVT) at 37 °C for 4 days, 1 week, and 2 weeks. (B) Schematic illustration and (C) an optical image of an aptamer-graphene microtransistor probe implanted into a mouse brain tissue. Blue spot indicates the approximate site of infusing dopamine solution. (D) Real-time response of an aptamer-graphene microtransistor probe implanted in the harvested mouse brain tissue upon the injection of dopamine solution (10 μM in aCSF, 2 μL). (E) Time-sequential sweeping of transfer curves when dopamine solution (10 μM in aCSF, 2 μL) was injected to the harvested brain tissue implanted with aptamer-graphene microtransistors. (F) The plot of source-drain current response upon the injection of dopamine solution (10 μM in aCSF, 2 μL) at V_g = 50 mV. (G) Image of a mouse implanted with a neural probe for monitoring the dopamine release evoked by pharmacological neuromodulation. (H) Representative response traces of aptamer-graphene microtransistors in the striatum after the local delivery of 60 mM potassium chloride (KCl, 0.5 μL) through the integrated microfluidic channel. (I) Representative response traces of aptamer-graphene microtransistors in the striatum after local delivery of 15 mM bicuculline (0.5 μL) through the integrated microfluidic channel. (J) The changes of electrical responses (compared with basal level) caused by the release of dopamine in the striatum upon KCl and bicuculline stimulations. Six data points from three mice in KCl experiments. Twelve data points from three mice in bicuculline experiments. The *in vivo* studies were performed 3 h after the implantation of neural probes. The influence of local infusion of (K) potassium chloride (60 mM) and (L) bicuculline (15 mM) on the performance of implantable aptamer-graphene microtransistors *in vitro*. V_{ds}= 100 mV, V_g = 50 mV.

microtransistors and gold-standard carbon fiber electrodes (with FSCV) to measure unknown dopamine levels in the aCSF solution. The dopamine concentration measured with aptamer-graphene microtransistors shows good agreement with those measured with FSCV, confirming the accurate measurements of physiologically relevant concentrations of dopamine in aCSF solution (Figure 3F).

Stability in CSF and *ex Vivo* Studies in Harvested Mice Brain Tissue. The developed neural probe needs to be stable in biological environments. Continuous exposure of the

https://doi.org/10.1021/acs.nanolett.2c00289
Nano Lett. XXXX, XXX, XXX−XXX

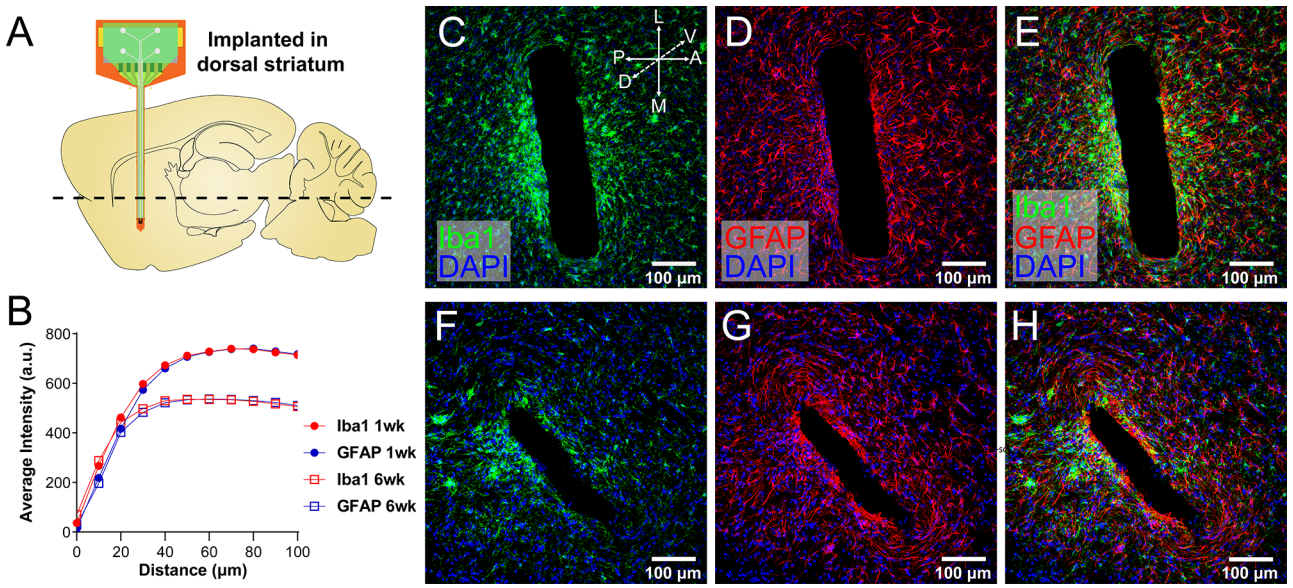

Figure 5. Impact of neural probe implantation on the mouse brain. (A) Schematic of neural probe implantation in the dorsal striatum. (B) Representative changes in intensity within ROI as the distance from device increases for both Iba1 (red) and GFAP (blue) at 1 week (closed circle) and 6 weeks (open square). (C–H) Representative confocal fluorescence images of horizontal striatal slices show immunohistochemical staining for DAPI (blue), astrocytes (GFAP, red), and activated microglia (Iba1, green) and overall lesion from neural probe implantation after 1 week (C–E) and 6 weeks (F–H). All histological and confocal settings were kept consistent across groups, 20× (Scale bars, 100 μm).

dopamine sensor to rat CSF (BioIVT) at 37 °C for 2 weeks produced stable concentration-dependent electrical responses at the physiologically relevant range of 1 nM to 10 μM dopamine (Figure 4A), suggesting the potential application for *in vivo* monitoring of dopamine. Nevertheless, various biofouling-resistant surface coatings, including polyethylene glycol (PEG) and its derivatives,[43] zwitterionic polymers,[44] or polyacrylamide hydrogels,[45] are needed to minimize the biofouling in a complicated *in vivo* environment for long-term monitoring. Furthermore, the covalent bonding between graphene and aptamers, through electrografting with diazonium salts[46] and EDC/NHS reactions,[47,48] is needed to enable the application in the complex biological environment. Therefore, this study focuses on short time dopamine monitoring in harvested brain tissue and in acute experiments.

We first tested the implantable aptamer-graphene microtransistors in harvested brain tissue from wild-type C57BL/6J mice (Figure 4B and C). The sensor response rapidly increases upon the infusion (10 μM, 2 μL) and diffusion of dopamine into the implantation site, to mimic evoked dopamine release, and then slowly decreases (Figure 4D). Similar results were obtained via continuously monitoring the transfer curves of aptamer-graphene microtransistors (Figure 4E and F). In our control experiments, the increases of sensor signal resulting from infusing aCSF (2 μL) are much smaller than those caused by dopamine infusion (Figure S2). These *ex vivo* studies in mice brain tissue illustrated the potential for monitoring dopamine release *in vivo*.

Real-Time Monitoring of Dopamine Release with Pharmacological Stimulation *in Vivo*. Motivated by the results of stability and *ex vivo* studies, we then monitored dopamine release evoked by local infusion of high concentration potassium or bicuculline through an integrated microfluidic channel in the striatum of the anesthetized mice (C57BL/6J) (Figure 4G). The determination of the absolute concentration of dopamine *in vivo* (i.e., basal concentrations) has been challenging due to the need of background subtraction for FSCV, though studies reported fast-scan controlled-adsorption voltammetry (FSCAV)[49] or the multiple square wave voltammetry (M-CSWV)[50] to get tonic levels of dopamine. For our implantable aptamer-graphene microtransistors, the complex biological environments could cause the inaccuracy of pre- and/or postcalibrations. Because of that, we report the sensor signal changes (compared with basal response) instead of absolute concentrations. This data analysis is consistent with other recently reported biosensors, including genetically fluorescent sensors[30,42] and aptamer-In_2O_3 field-effect transistors,[18] for real-time monitoring of dopamine and/or serotonin release *in vivo*, in which a change of fluorescent signals or calibrated field-effect transistor response was reported.

In our study, the neural probe with an integrated microfluidic channel was first implanted into the striatum. Three hours later, KCl or bicuculline (0.5 μL; 60 mM KCl or 15 mM bicuculline) was delivered at a flow rate of 0.5 μL/min for 1 min through the integrated microfluidic channels. Bicuculline, a GABA antagonist, can competitively antagonize the inhibition of the target neurons, as a result, promoting dopamine release.[51,52] A customized amplifier circuit was designed to integrate with the neural probe for *in vivo* monitoring dopamine release (Figures S3–S6). After 60 s application of 60 mM K^+ or 15 mM bicuculline, a rapid change of the sensor signal was observed, and the signal rapidly vanished within several seconds (Figure 4H–J), indicating that the implantable aptamer-graphene microtransistors with a dopamine-specific aptamer detected the release of dopamine after K^+ or bicuculline stimulation. To assess the influence of local fluid delivery on the performance of aptamer-graphene microtransistors, we studied the sensor signal change upon the local delivery of potassium chloride (60 mM) or bicuculline (15 mM) *in vitro* to aptamer-graphene microtransistors (Figure 4K and L). Minimal sensor signal changes were observed, indicating the transient sensor signal changes in Figure 4H and I are caused by the dopamine release instead of the sensor

https://doi.org/10.1021/acs.nanolett.2c00289
Nano Lett. XXXX, XXX, XXX–XXX

interferences. We did not validate the evoked release of dopamine *in vivo* using FSCV due to the technical challenge of implanting aptamer-graphene microtransistors or microfluidics with gold-standard carbon fibers in the same brain site (striatum). Overall, these studies indicate the capability of neural probes for monitoring dopamine release *in vivo*.

Distinct from the electrolyte-gated graphene microtransistors that rely on the modulation of channel resistance of graphene by an electrophysiological signal through the gate-electrolyte capacitance,[25] our implantable aptamer functionalized graphene microtransistors rely on the conformational rearrangement of aptamers in the presence of target neurochemical, which results in the increase/decrease of carriers (electron or hole) in the graphene channel. In addition, the electrophysiological signals and neurochemical release can be distinguished due to the different time scales (~100 ms vs several seconds) (Figure 4H and I, Figure S7).

Finally, to assess the influence of device implantation on brain tissue, the neural probes were implanted for 1 week and 6 weeks in the dorsal striatum of mice (Figure 5A). Using the same confocal microscope settings, we determined that the immune response for astrocytes and activated microglia at 1 week and 6 weeks (Figure 5B). These results suggest that the immune response to device implantation decreases over time (Figures 5C−H). In addition, the immune response and area of lesion tissue caused by our neural probes are consistent with those induced by other state-of-art thin-film deep brain implants.[53−55]

DISCUSSION AND CONCLUSION

In summary, the implantable neural probe demonstrated here delivers an adaptable technical platform for dopamine monitoring with high sensitivity (10 pM for dopamine), molecular specificity (dopamine sensor: >19-fold over norepinephrine), and spatiotemporal precision (nearly cellular scale; 2.09 s on time and 5.38 s off time). The reversibility and high spatiotemporal resolution allow for the real-time monitoring of transient fluctuations of dopamine concentrations at the cellular level *in vivo*. Furthermore, the *in vivo* studies in mice model demonstrate the real-time monitoring of dopamine release evoked by pharmacological stimulation, creating new opportunities to study neurochemically driven changes in behaviors or neural activities. Our neural probe is distinct from the recently reported implantable aptamer-In_2O_3-FET for monitoring serotonin[18] in two ways: (1) Different from the aptamer-In_2O_3-FET that is reported to monitor serotonin, we demonstrate the real-time monitoring of pharmacological stimulation evoked dopamine release *in vivo*. (2) Our implantable aptamer-graphene microtransistors use graphene as the channel layer, which has a much higher carrier mobility of 1370.18 $cm^2/V{\cdot}s$ than that of In_2O_3 (17.8 ± 1.8 $cm^2/V{\cdot}s$).[18,19] Areas for future development include (1) investigating various surface coatings[43−45] to minimize the biofouling for long-term monitoring in freely moving animals, (2) detecting the release of dopamine in nucleus accumbens (NAc) upon the optogenetic stimulation of ventral tegmental area (VTA) for DAT-Cre mice expressing ChR2,[56] and (3) validating the dopamine release in NAc using FSCV or genetically encoded fluorescent dopamine sensors.

ASSOCIATED CONTENT

Supporting Information

The Supporting Information is available free of charge at https://pubs.acs.org/doi/10.1021/acs.nanolett.2c00289.

Materials and methods, carrier mobility calculation, amplifier circuit, summary of representative technologies for *in vivo* neurochemical monitoring, schematic illustration for the fabrication of graphene microtransistors, ex vivo studies of implantable aptamer-graphene microtransistors in the harvested mouse brain tissue upon the injection of 2 μL aCSF, schematic illustration of the amplification circuit, circuit simplification, constructed circuit, TL082CP dual JFET-input operational amplifier pinout, and real-time monitoring of dopamine release with pharmacological stimulation *in vivo* in the striatum of mice. (PDF)

AUTHOR INFORMATION

Corresponding Author

Yi Zhang − *Department of Biomedical Engineering and the Institute of Materials Science, University of Connecticut, Storrs, Connecticut 06269, United States;* orcid.org/0000-0002-0907-663X; Email: yi.5.zhang@uconn.edu

Authors

Guangfu Wu − *Department of Biomedical Engineering and the Institute of Materials Science, University of Connecticut, Storrs, Connecticut 06269, United States*

Nannan Zhang − *Dalton Cardiovascular Research Center, University of Missouri, Columbia, Missouri 65211, United States*

Avi Matarasso − *Department of Bioengineering, University of Washington, Seattle, Washington 98195, United States*

Ian Heck − *Department of Biomedical, Biological, and Chemical Engineering, University of Missouri, Columbia, Missouri 65211, United States*

Huijie Li − *Department of Biomedical Engineering and the Institute of Materials Science, University of Connecticut, Storrs, Connecticut 06269, United States*

Wei Lu − *Department of Materials Science and Engineering and Center for Bio-Integrated Electronics, Northwestern University, Evanston, Illinois 60208, United States*

J. Glenn Phaup − *Center for Precision Medicine, University of Missouri, Columbia, Missouri 65212, United States*

Michael J. Schneider − *Department of Biomedical Engineering and the Institute of Materials Science, University of Connecticut, Storrs, Connecticut 06269, United States*

Yixin Wu − *Department of Materials Science and Engineering and Center for Bio-Integrated Electronics, Northwestern University, Evanston, Illinois 60208, United States*

Zhengyan Weng − *Department of Biomedical Engineering and the Institute of Materials Science, University of Connecticut, Storrs, Connecticut 06269, United States*

He Sun − *Department of Biomedical Engineering and the Institute of Materials Science, University of Connecticut, Storrs, Connecticut 06269, United States*

Zan Gao − *Department of Biomedical Engineering and the Institute of Materials Science, University of Connecticut, Storrs, Connecticut 06269, United States*

Xincheng Zhang − *Department of Biomedical Engineering and the Institute of Materials Science, University of Connecticut, Storrs, Connecticut 06269, United States*

https://doi.org/10.1021/acs.nanolett.2c00289
Nano Lett. XXXX, XXX, XXX−XXX

Stefan G. Sandberg − *Department of Psychiatry and Behavioral Sciences, University of Washington, Seattle, Washington 98195, United States*
Dilruba Parvin − *Department of Electrical Engineering and Computer Science, University of Missouri, Columbia, Missouri 65211, United States*
Elena Seaholm − *Department of Bioengineering, University of Washington, Seattle, Washington 98195, United States*
Syed Kamrul Islam − *Department of Electrical Engineering and Computer Science, University of Missouri, Columbia, Missouri 65211, United States*
Xueju Wang − *Department of Materials Science and Engineering and the Institute of Materials Science, University of Connecticut, Storrs, Connecticut 06269, United States;* orcid.org/0000-0002-0669-8759
Paul E. M. Phillips − *Department of Psychiatry and Behavioral Sciences, University of Washington, Seattle, Washington 98195, United States*
Daniel C. Castro − *Department of Anesthesiology and Pain Medicine, University of Washington, Seattle, Washington 98195,, United States; Center for Neurobiology of Addiction, Pain, and Emotion and Department of Pharmacology, University of Washington, Seattle, Washington 98195, United States*
Shinghua Ding − *Dalton Cardiovascular Research Center, University of Missouri, Columbia, Missouri 65211, United States; Department of Biomedical, Biological, and Chemical Engineering, University of Missouri, Columbia, Missouri 65211, United States*
De-Pei Li − *Center for Precision Medicine, University of Missouri, Columbia, Missouri 65212, United States*
Michael R. Bruchas − *Department of Bioengineering, University of Washington, Seattle, Washington 98195, United States; Department of Anesthesiology and Pain Medicine, University of Washington, Seattle, Washington 98195,, United States; Center for Neurobiology of Addiction, Pain, and Emotion and Department of Pharmacology, University of Washington, Seattle, Washington 98195, United States*

Complete contact information is available at: https://pubs.acs.org/10.1021/acs.nanolett.2c00289

Author Contributions

G.W. and Y.Z. conceived of the idea and designed the experiments; I.H., W.L., D.P., S.K.I., and X.Z. discussed and designed the amplifier circuit; G.W. designed and fabricated aptamer-graphene microtransistors; Y.W., H.L., Z.W., H.S., and Z.G. contributed to device fabrication and assembly; G.W., N.Z., J.G.P., S.D., and D.L. designed and performed surgical implantations and recorded the data of real-time dopamine detection in mouse brain; MS collected brain tissue for *ex vivo* studies; S.S. and P.E.M.P. contributed to the discussion on FSCV technology; M.R.B. provided guidance regarding the design requirements of neural probes; A.M., E.S., D.C.C., and M.R.B. performed immunohistochemistry; G.W., N.Z., I.H., A.M., X.W., and Y.Z. wrote the manuscript. All authors discussed the results and contributed to the final manuscript.

Funding

Y.Z. is supported by the University of Connecticut start-up fund, NIH RF1NS118287, NIH R42MH116525, and NIH R61DA051489. S.D. is supported by NIH R01NS069726 and R01NS094539. DPL is supported by NIH R01HL139523 and R01HL142133. P.E.M.P. and S.S. are supported by NIH R01DA039687 and R37DA051686.

Notes

The authors declare no competing financial interest.

■ ACKNOWLEDGMENTS

We would like to thank the Institute of Molecular and Nanoscale Innovation (IMNI) at Brown University for access to Nanofabrication Central Facility (NCF). This work used NCF for fabricating graphene microtransistors.

■ REFERENCES

(1) Steinmetz, N. A.; Aydin, C.; Lebedeva, A.; Okun, M.; Pachitariu, M.; Bauza, M.; Beau, M.; Bhagat, J.; Bohm, C.; Broux, M.; Chen, S.; Colonell, J.; Gardner, R. J.; Karsh, B.; Kloosterman, F.; Kostadinov, D.; Mora-Lopez, C.; O'Callaghan, J.; Park, J.; Putzeys, J.; Sauerbrei, B.; van Daal, R. J. J.; Vollan, A. Z.; Wang, S.; Welkenhuysen, M.; Ye, Z.; Dudman, J. T.; Dutta, B.; Hantman, A. W.; Harris, K. D.; Lee, A. K.; Moser, E. I.; O'Keefe, J.; Renart, A.; Svoboda, K.; Hausser, M.; Haesler, S.; Carandini, M.; Harris, T. D. Neuropixels 2.0: A miniaturized high-density probe for stable, long-term brain recordings. *Science* **2021**, *372* (6539), No. eabf4588.
(2) Chiang, C. H.; Won, S. M.; Orsborn, A. L.; Yu, K. J.; Trumpis, M.; Bent, B.; Wang, C.; Xue, Y.; Min, S.; Woods, V.; Yu, C.; Kim, B. H.; Kim, S. B.; Huq, R.; Li, J.; Seo, K. J.; Vitale, F.; Richardson, A.; Fang, H.; Huang, Y.; Shepard, K.; Pesaran, B.; Rogers, J. A.; Viventi, J. Development of a neural interface for high-definition, long-term recording in rodents and nonhuman primates. *Sci. Transl Med.* **2020**, *12* (538), No. eaay4682.
(3) Wise, R. A. Dopamine, learning and motivation. *Nat. Rev. Neurosci* **2004**, *5* (6), 483−94.
(4) Holroyd, C. B.; Coles, M. G. H. The neural basis of human error processing: reinforcement learning, dopamine, and the error-related negativity. *Psychol Rev.* **2002**, *109* (4), 679−709.
(5) Mohebi, A.; Pettibone, J. R.; Hamid, A. A.; Wong, J. T.; Vinson, L. T.; Patriarchi, T.; Tian, L.; Kennedy, R. T.; Berke, J. D. Dissociable dopamine dynamics for learning and motivation. *Nature* **2019**, *570* (7759), 65−70.
(6) Graybiel, A. M.; Aosaki, T.; Flaherty, A. W.; Kimura, M. The basal ganglia and adaptive motor control. *Science* **1994**, *265* (5180), 1826−31.
(7) Lotharius, J.; Brundin, P. Pathogenesis of Parkinson's disease: dopamine, vesicles and alpha-synuclein. *Nat. Rev. Neurosci* **2002**, *3* (12), 932−42.
(8) Segura-Aguilar, J.; Paris, I.; Munoz, P.; Ferrari, E.; Zecca, L.; Zucca, F. A. Protective and toxic roles of dopamine in Parkinson's disease. *J. Neurochem* **2014**, *129* (6), 898−915.
(9) Howes, O. D.; Kapur, S. The dopamine hypothesis of schizophrenia: version III-the final common pathway. *Schizophr Bull.* **2009**, *35* (3), 549−62.
(10) Robinson, D. L.; Hermans, A.; Seipel, A. T.; Wightman, R. M. Monitoring rapid chemical communication in the brain. *Chem. Rev.* **2008**, *108* (7), 2554−84.
(11) Frank, J. A.; Antonini, M. J.; Anikeeva, P. Next-generation interfaces for studying neural function. *Nat. Biotechnol.* **2019**, *37* (9), 1013−1023.
(12) Tan, C.; Robbins, E. M.; Wu, B.; Cui, X. T. Recent Advances in In Vivo Neurochemical Monitoring. *Micromachines (Basel)* **2021**, *12* (2), 208.
(13) Zhang, Y.; Jiang, N.; Yetisen, A. K. Brain neurochemical monitoring. *Biosens Bioelectron* **2021**, *189*, 113351.
(14) Ngernsutivorakul, T.; White, T. S.; Kennedy, R. T. Microfabricated Probes for Studying Brain Chemistry: A Review. *ChemPhysChem* **2018**, *19* (10), 1128−1142.
(15) Sim, J. Y.; Haney, M. P.; Park, S. I.; McCall, J. G.; Jeong, J. W. Microfluidic neural probes: in vivo tools for advancing neuroscience. *Lab Chip* **2017**, *17* (8), 1406−1435.

(16) Gu, H.; Varner, E. L.; Groskreutz, S. R.; Michael, A. C.; Weber, S. G. In Vivo Monitoring of Dopamine by Microdialysis with 1 min Temporal Resolution Using Online Capillary Liquid Chromatography with Electrochemical Detection. *Anal. Chem.* **2015**, *87* (12), 6088−94.
(17) Xie, K.; Wang, N.; Lin, X.; Wang, Z.; Zhao, X.; Fang, P.; Yue, H.; Kim, J.; Luo, J.; Cui, S. Organic electrochemical transistor arrays for real-time mapping of evoked neurotransmitter release in vivo. *Elife* **2020**, *9*, No. e50345.
(18) Zhao, C.; Cheung, K. M.; Huang, I. W.; Yang, H.; Nakatsuka, N.; Liu, W.; Cao, Y.; Man, T.; Weiss, P. S.; Monbouquette, H. G.; Andrews, A. M. Implantable aptamer-field-effect transistor neuroprobes for in vivo neurotransmitter monitoring. *Sci. Adv.* **2021**, *7* (48), No. eabj7422.
(19) Liu, Q.; Zhao, C.; Chen, M.; Liu, Y.; Zhao, Z.; Wu, F.; Li, Z.; Weiss, P. S.; Andrews, A. M.; Zhou, C. Flexible Multiplexed In2O3 Nanoribbon Aptamer-Field-Effect Transistors for Biosensing. *iScience* **2020**, *23* (9), 101469.
(20) Gao, N.; Gao, T.; Yang, X.; Dai, X.; Zhou, W.; Zhang, A.; Lieber, C. M. Specific detection of biomolecules in physiological solutions using graphene transistor biosensors. *Proc. Natl. Acad. Sci. U. S. A.* **2016**, *113* (51), 14633−14638.
(21) Fu, W.; Jiang, L.; van Geest, E.; Lima, L.; Schneider, G. Sensing at the surface of graphene field-effect transistors. *Adv. Mater.* **2017**, *29* (6), 1603610.
(22) Hwang, M. T.; Heiranian, M.; Kim, Y.; You, S.; Leem, J.; Taqieddin, A.; Faramarzi, V.; Jing, Y.; Park, I.; van der Zande, A. M. Ultrasensitive detection of nucleic acids using deformed graphene channel field effect biosensors. *Nat. Commun.* **2020**, *11* (1), 1−11.
(23) Béraud, A.; Sauvage, M.; Bazán, C. M.; Tie, M.; Bencherif, A.; Bouilly, D. Graphene field-effect transistors as bioanalytical sensors: Design, operation and performance. *Analyst* **2021**, *146* (2), 403−428.
(24) Bonaccini Calia, A.; Masvidal-Codina, E.; Smith, T. M.; Schafer, N.; Rathore, D.; Rodriguez-Lucas, E.; Illa, X.; De la Cruz, J. M.; Del Corro, E.; Prats-Alfonso, E.; Viana, D.; Bousquet, J.; Hebert, C.; Martinez-Aguilar, J.; Sperling, J. R.; Drummond, M.; Halder, A.; Dodd, A.; Barr, K.; Savage, S.; Fornell, J.; Sort, J.; Guger, C.; Villa, R.; Kostarelos, K.; Wykes, R. C.; Guimera-Brunet, A.; Garrido, J. A. Full-bandwidth electrophysiology of seizures and epileptiform activity enabled by flexible graphene microtransistor depth neural probes. *Nat. Nanotechnol* **2022**, *17* (3), 301−309.
(25) Masvidal-Codina, E.; Illa, X.; Dasilva, M.; Calia, A. B.; Dragojevic, T.; Vidal-Rosas, E. E.; Prats-Alfonso, E.; Martinez-Aguilar, J.; De la Cruz, J. M.; Garcia-Cortadella, R.; Godignon, P.; Rius, G.; Camassa, A.; Del Corro, E.; Bousquet, J.; Hebert, C.; Durduran, T.; Villa, R.; Sanchez-Vives, M. V.; Garrido, J. A.; Guimera-Brunet, A. High-resolution mapping of infraslow cortical brain activity enabled by graphene microtransistors. *Nat. Mater.* **2019**, *18* (3), 280−288.
(26) Hébert, C.; Masvidal-Codina, E.; Suarez-Perez, A.; Calia, A. B.; Piret, G.; Garcia-Cortadella, R.; Illa, X.; Del Corro Garcia, E.; De la Cruz Sanchez, J. M.; Casals, D. V. Flexible graphene solution-gated field-effect transistors: efficient transducers for micro-electrocorticography. *Adv. Funct. Mater.* **2018**, *28* (12), 1703976.
(27) Hwang, M. T.; Park, I.; Heiranian, M.; Taqieddin, A.; You, S.; Faramarzi, V.; Pak, A. A.; van der Zande, A. M.; Aluru, N. R.; Bashir, R. Ultrasensitive Detection of Dopamine, IL-6 and SARS-CoV-2 Proteins on Crumpled Graphene FET Biosensor. *Adv. Mater. Technol.* **2021**, *6* (11), 2100712.
(28) Abrantes, M.; Rodrigues, D.; Domingues, T.; Nemala, S. S.; Monteiro, P.; Borme, J.; Alpuim, P.; Jacinto, L., Ultrasensitive Dopamine Detection with Graphene Aptasensor Multitransistor Arrays. *bioRxiv* **2022**, *Preprint* (March 6, 2022), DOI: 10.1101/2022.03.04.483061.
(29) Zachek, M. K.; Park, J.; Takmakov, P.; Wightman, R. M.; McCarty, G. S. Microfabricated FSCV-compatible microelectrode array for real-time monitoring of heterogeneous dopamine release. *Analyst* **2010**, *135* (7), 1556−63.
(30) Patriarchi, T.; Cho, J. R.; Merten, K.; Howe, M. W.; Marley, A.; Xiong, W. H.; Folk, R. W.; Broussard, G. J.; Liang, R.; Jang, M. J.; Zhong, H.; Dombeck, D.; von Zastrow, M.; Nimmerjahn, A.; Gradinaru, V.; Williams, J. T.; Tian, L. Ultrafast neuronal imaging of dopamine dynamics with designed genetically encoded sensors. *Science* **2018**, *360* (6396), No. eaat4422.
(31) Nakatsuka, N.; Yang, K. A.; Abendroth, J. M.; Cheung, K. M.; Xu, X.; Yang, H.; Zhao, C.; Zhu, B.; Rim, Y. S.; Yang, Y.; Weiss, P. S.; Stojanovic, M. N.; Andrews, A. M. Aptamer-field-effect transistors overcome Debye length limitations for small-molecule sensing. *Science* **2018**, *362* (6412), 319−324.
(32) Blind, M.; Blank, M. Aptamer Selection Technology and Recent Advances. *Mol. Ther Nucleic Acids* **2015**, *4*, No. e223.
(33) Dhiman, D.; Kalra, P.; Bansal, V.; Bruno, J.; Sharma, T. Aptamer-based point-of-care diagnostic platforms. *Sens. Actuators, B* **2017**, *246*, 535−553.
(34) Shin, G.; Gomez, A. M.; Al-Hasani, R.; Jeong, Y. R.; Kim, J.; Xie, Z.; Banks, A.; Lee, S. M.; Han, S. Y.; Yoo, C. J.; Lee, J. L.; Lee, S. H.; Kurniawan, J.; Tureb, J.; Guo, Z.; Yoon, J.; Park, S. I.; Bang, S. Y.; Nam, Y.; Walicki, M. C.; Samineni, V. K.; Mickle, A. D.; Lee, K.; Heo, S. Y.; McCall, J. G.; Pan, T.; Wang, L.; Feng, X.; Kim, T. I.; Kim, J. K.; Li, Y.; Huang, Y.; Gereau, R. W. t.; Ha, J. S.; Bruchas, M. R.; Rogers, J. A. Flexible Near-Field Wireless Optoelectronics as Subdermal Implants for Broad Applications in Optogenetics. *Neuron* **2017**, *93* (3), 509−521 e3.
(35) Lu, L.; Gutruf, P.; Xia, L.; Bhatti, D. L.; Wang, X.; Vazquez-Guardado, A.; Ning, X.; Shen, X.; Sang, T.; Ma, R.; Pakeltis, G.; Sobczak, G.; Zhang, H.; Seo, D. O.; Xue, M.; Yin, L.; Chanda, D.; Sheng, X.; Bruchas, M. R.; Rogers, J. A. Wireless optoelectronic photometers for monitoring neuronal dynamics in the deep brain. *Proc. Natl. Acad. Sci. U. S. A.* **2018**, *115* (7), E1374−E1383.
(36) Gilletti, A.; Muthuswamy, J. Brain micromotion around implants in the rodent somatosensory cortex. *J. Neural Eng.* **2006**, *3* (3), 189−95.
(37) Wu, G. D. Z.; Tang, X.; Lin, Z.; Lo, P.; Meyyappan, M.; Lai, K. Graphene Field-Effect Transistors for the Sensitive and Selective Detection of Escherichia coli Using Pyrene-Tagged DNA Aptamer. *Adv. Healthcare Mater.* **2017**, *6* (19), 1700736.
(38) Wu, G. T. X.; Meyyappan, M.; Lai, K. Doping effects of surface functionalization on graphene with aromatic molecule and organic solvents. *Appl. Surf. Sci.* **2017**, *425*, 713−721.
(39) Ferguson, B. S.; Hoggarth, D. A.; Maliniak, D.; Ploense, K.; White, R. J.; Woodward, N.; Hsieh, K.; Bonham, A. J.; Eisenstein, M.; Kippin, T. E.; Plaxco, K. W.; Soh, H. T. Real-time, aptamer-based tracking of circulating therapeutic agents in living animals. *Sci. Transl Med.* **2013**, *5* (213), 213ra165.
(40) Wilson, B. D.; Hariri, A. A.; Thompson, I. A. P.; Eisenstein, M.; Soh, H. T. Independent control of the thermodynamic and kinetic properties of aptamer switches. *Nat. Commun.* **2019**, *10* (1), 5079.
(41) Clark, J. J.; Sandberg, S. G.; Wanat, M. J.; Gan, J. O.; Horne, E. A.; Hart, A. S.; Akers, C. A.; Parker, J. G.; Willuhn, I.; Martinez, V.; Evans, S. B.; Stella, N.; Phillips, P. E. M. Chronic microsensors for longitudinal, subsecond dopamine detection in behaving animals. *Nat. Methods* **2010**, *7* (2), 126−129.
(42) Sun, F.; Zeng, J.; Jing, M.; Zhou, J.; Feng, J.; Owen, S. F.; Luo, Y.; Li, F.; Wang, H.; Yamaguchi, T.; Yong, Z.; Gao, Y.; Peng, W.; Wang, L.; Zhang, S.; Du, J.; Lin, D.; Xu, M.; Kreitzer, A. C.; Cui, G.; Li, Y. A Genetically Encoded Fluorescent Sensor Enables Rapid and Specific Detection of Dopamine in Flies, Fish, and Mice. *Cell* **2018**, *174* (2), 481−496 e19.
(43) Lowe, S.; O'Brien-Simpson, N. M.; Connal, L. A. Antibiofouling polymer interfaces: poly (ethylene glycol) and other promising candidates. *Polym. Chem.* **2015**, *6* (2), 198−212.
(44) Golabchi, A.; Wu, B.; Cao, B.; Bettinger, C. J.; Cui, X. T. Zwitterionic polymer/polydopamine coating reduce acute inflammatory tissue responses to neural implants. *Biomaterials* **2019**, *225*, 119519.
(45) Chan, D.; Chien, J.-C.; Axpe, E.; Blankemeier, L.; Baker, S. W.; Swaminathan, S.; Piunova, V. A.; Zubarev, D. Y.; Maikawa, C. L.; Grosskopf, A. K. Combinatorial polyacrylamide hydrogels for preventing biofouling on implantable biosensors. *BioRxiv* **2021**,

https://doi.org/10.1021/acs.nanolett.2c00289
Nano Lett. XXXX, XXX, XXX−XXX

Preprint (October 3, 2021, Version 4), DOI: 10.1101/2020.05.25.115675.
(46) Paulus, G. L.; Wang, Q. H.; Strano, M. S. Covalent electron transfer chemistry of graphene with diazonium salts. *Acc. Chem. Res.* **2013**, *46* (1), 160−70.
(47) Wang, C.; Yan, Q.; Liu, H. B.; Zhou, X. H.; Xiao, S. J. Different EDC/NHS activation mechanisms between PAA and PMAA brushes and the following amidation reactions. *Langmuir* **2011**, *27* (19), 12058−68.
(48) Wickramathilaka, M. P.; Tao, B. Y. Characterization of covalent crosslinking strategies for synthesizing DNA-based bioconjugates. *J. Biol. Eng.* **2019**, *13*, 63.
(49) Atcherley, C. W.; Wood, K. M.; Parent, K. L.; Hashemi, P.; Heien, M. L. The coaction of tonic and phasic dopamine dynamics. *Chem. Commun. (Camb)* **2015**, *51* (12), 2235−8.
(50) Oh, Y.; Heien, M. L.; Park, C.; Kang, Y. M.; Kim, J.; Boschen, S. L.; Shin, H.; Cho, H. U.; Blaha, C. D.; Bennet, K. E.; Lee, H. K.; Jung, S. J.; Kim, I. Y.; Lee, K. H.; Jang, D. P. Tracking tonic dopamine levels in vivo using multiple cyclic square wave voltammetry. *Biosens Bioelectron* **2018**, *121*, 174−182.
(51) Karreman, M.; Moghaddam, B. The prefrontal cortex regulates the basal release of dopamine in the limbic striatum: an effect mediated by ventral tegmental area. *J. Neurochem* **1996**, *66* (2), 589−98.
(52) Smolders, I.; De Klippel, N.; Sarre, S.; Ebinger, G.; Michotte, Y. Tonic GABA-ergic modulation of striatal dopamine release studied by in vivo microdialysis in the freely moving rat. *Eur. J. Pharmacol.* **1995**, *284* (1−2), 83−91.
(53) Canales, A.; Jia, X.; Froriep, U. P.; Koppes, R. A.; Tringides, C. M.; Selvidge, J.; Lu, C.; Hou, C.; Wei, L.; Fink, Y.; Anikeeva, P. Multifunctional fibers for simultaneous optical, electrical and chemical interrogation of neural circuits in vivo. *Nat. Biotechnol.* **2015**, *33* (3), 277−84.
(54) Jeong, J. W.; McCall, J. G.; Shin, G.; Zhang, Y.; Al-Hasani, R.; Kim, M.; Li, S.; Sim, J. Y.; Jang, K. I.; Shi, Y.; Hong, D. Y.; Liu, Y.; Schmitz, G. P.; Xia, L.; He, Z.; Gamble, P.; Ray, W. Z.; Huang, Y.; Bruchas, M. R.; Rogers, J. A. Wireless Optofluidic Systems for Programmable In Vivo Pharmacology and Optogenetics. *Cell* **2015**, *162* (3), 662−74.
(55) Zhang, Y.; Castro, D. C.; Han, Y.; Wu, Y.; Guo, H.; Weng, Z.; Xue, Y.; Ausra, J.; Wang, X.; Li, R.; Wu, G.; Vazquez-Guardado, A.; Xie, Y.; Xie, Z.; Ostojich, D.; Peng, D.; Sun, R.; Wang, B.; Yu, Y.; Leshock, J. P.; Qu, S.; Su, C. J.; Shen, W.; Hang, T.; Banks, A.; Huang, Y.; Radulovic, J.; Gutruf, P.; Bruchas, M. R.; Rogers, J. A. Battery-free, lightweight, injectable microsystem for in vivo wireless pharmacology and optogenetics. *Proc. Natl. Acad. Sci. U. S. A.* **2019**, *116* (43), 21427−21437.
(56) Tsai, H. C.; Zhang, F.; Adamantidis, A.; Stuber, G. D.; Bonci, A.; de Lecea, L.; Deisseroth, K. Phasic firing in dopaminergic neurons is sufficient for behavioral conditioning. *Science* **2009**, *324* (5930), 1080−4.

https://doi.org/10.1021/acs.nanolett.2c00289
Nano Lett. XXXX, XXX, XXX−XXX